Optimal Temperature and Current Cycles for Curing of Composites Using Embedded Resistive Heating Elements

A. Mawardi

R. Pitchumani
e-mail: r.pitchumani@uconn.edu

Composites Processing Laboratory,
Department of Mechanical Engineering,
University of Connecticut,
Storrs, CT 06269-3139

*Curing is an important and time consuming step in the fabrication of thermosetting-matrix composite products. The use of embedded resistive heating elements providing supplemental heating from within the material being cured has been shown in previous studies (Ramakrishnan, Zhu, and Pitchumani, 2000, J. Manuf. Sci. Eng., **122**, pp. 124–131; and Zhu and Pitchumani, 2000, Compos. Sci. Technol., **60**, 2699–2712.) to offer significant improvements in cure cycle time and cure uniformity, due to the inside-out curing. This paper addresses the problem of determining the temperature and electrical current cycles, as well as the placement configuration of the conductive mats, for time-optimal curing of composites using embedded resistive heating elements. A continuous search simulated annealing optimization technique is utilized coupled with a numerical process simulation model to determine the optimal solutions for selected process constraints. Optimization results are presented over a range of material systems and different numbers of conductive mats to assess the effects of materials reactivity on the optimal number of conductive mats.* [DOI: 10.1115/1.1527903]

Keywords: Composites Fabrication, Optimal Cure Cycles, Heat Transfer, Resin Transfer Molding, Resistive Heating

1 Introduction

Fabrication of thermosetting-matrix composites is accomplished by subjecting the resin-fiber mixture to a prescribed temperature cycle in order to initiate and sustain an irreversible crosslinking exothermic chemical reaction in the resin, called cure. The cure process causes the initial mixture to be transformed into a rigid component whose structural integrity is retained upon the withdrawal of the external temperature variation. The magnitude and time duration of the imposed temperature variation, referred to as the cure cycle, is an important process parameter affecting the temperature distribution and the progress of the crosslinking reaction (measured in terms of a degree of cure) within the composite.

Initially during the cure process, the temperature of the outer layers of the composite which are exposed to the cure temperature cycle increases more rapidly than that of the inner layers, and as the process progresses, the exothermic cure reaction may bring the temperatures of the inner layers to exceed those of the outer layers. Moreover, the heat released during the cure reaction may lead to excessively rapid rate of temperature increase, or the temperature within the material exceeding an allowable maximum value. Maintaining spatial homogeneity in the temperature and degree of cure distribution within the matrix, and maintaining the exotherm-induced maximum temperature and temperature gradient within allowable limits constitute the principal constraints governing the total time of the cure process.

Determination of cure cycles that lead to minimum cure time in practice has relied on trial-and-error or empirical procedure where either simulations based on numerical models or experimental trials are carried out for several candidate cure cycles (Pillai et al. [3]; Loos and Springer [4]; Han et al. [5]; Bogetti and Gillespie [6]; Ciriscioli et al. [7]). This approach does not warrant the best possible process parameters, and, in turn, leads to suboptimal manufacturing times and cost. A rigorous approach to determining the optimal cure cycle was reported by Rai and Pitchumani [8], in which an optimization problem was formulated over a numerical process model and solved using a nonlinear programming scheme. The results were reported for a wide range of resin materials and process constraints. It was shown that the constraints on temperature and cure homogeneity fundamentally limit the magnitude of the temperature ramps in the optimal cycles. This constitutes a fundamental limitation of the curing of composites using peripheral heating.

The foregoing limitation may be alleviated via an inside-out curing strategy, where the inner layers are also subjected to a heat source that allows them to cure in synchronization with the outer layers. Such a strategy provides for temperature and cure homogeneity through the composite cross section during the cure process, and in turn offers the potential to significantly reduce the cure time. One approach toward realizing volumetric internal heating is the use of microwave energy (Lee and Springer [9]; Thostensen and Chou [10]). This approach provides improvement to conventional curing; however, the problem of differential curing persists since the microwave energy attenuates with thickness.

The objective of inside-out curing may also be realized through the use of conductive carbon fibers as resistive heating elements embedded within the cross-section of the composite being cured. Ramakrishnan et al. [1] and Zhu and Pitchumani [2] investigated the approach numerically and experimentally for several resistive heating configurations and demonstrated improved temperature and cure homogeneity, and significant savings in the cure time. The investigation focused on a prescribed cure temperature cycle while varying the steady current supplied to the resistive heating elements. It may be envisioned that significant enhancement to the process could be realized through the use of a time varying current cycle, whereby the current supplied may be better tailored to accelerating the process. In this case, process design calls for determination of the optimal temperature and current variations during the process, which is the focus of the present study.

Contributed by the Heat Transfer Division for publication in the JOURNAL OF HEAT TRANSFER. Manuscript received by the Heat Transfer Division March 21, 2001; revision received August 12, 2002. Associate Editor: A. F. Emery.

Specifically, this paper considers the problem of determining the optimal cure temperature and current cycles so as to minimize the fabrication time while simultaneously satisfying constraints on (a) the maximum material temperature, $T_{\max}$, (b) the maximum temperature gradient, $\dot{T}_{\max}$, (c) the maximum temperature difference across the material, $\Delta T_{\max}$, and (d) the minimum degree of cure desired in the product, $\epsilon_{\min}$. The decision variables consist of the magnitude and duration of each stage of the temperature cycle prescribed in the peripheral heating, the magnitudes and durations of the stages of the electrical current cycles in the resistive heating elements, and the location of the heating elements within the laminates. The optimization problem is solved using a simplex search based simulated annealing algorithm, combined with a numerical process simulation model to obtain both objective function and constraints information. The optimization results are presented for selected process constraints on three different resin systems.

The paper is organized as follows: The process model development is presented in Section 2, followed by the formulation of the optimization problem in Section 3. Section 4 discusses the optimization results along with the parametric studies.

2 Process Model

Figure 1 shows a schematic description of a process configuration with embedded resistive heating elements. The configuration consists of a lay-up of resin saturated fiber layers placed between two tooling plates. Interspersed among the fiber layers are discrete layers of conductive-fiber mats, placed at specific locations across the thickness, where electrical current is passed through to produce resistive heating along those discrete planes within the cross section. Peripheral heating with prescribed temperature cycle is applied from the bottom plate, while the top plate surface is exposed to the surrounding allowing heat transfer through convection.

Heat transfer takes effect from the cure temperature cycle imposed on the bottom plate as well as from resistive heating elements embedded in the cross-section. The cure reaction proceeds simultaneously with the heating of the material, and the exothermic nature of the cure reaction generates heat which in turn helps to accelerate further reaction. The dominant physical phenomena in the process are (a) heat transfer associated with the heating from the bottom plate as well as volumetric heating due to the resistive heating at the conductive mats including the exothermic cure reaction, and (b) the chemical reaction leading the cure process.

Mathematical models for the process are formulated from energy conservation and chemical kinetics considerations. The energy transfer is assumed to be predominantly one-dimensional through the thickness of the layers (y-direction in Fig. 1), since the surface and resistive heating are uniform along the length-width plane of the layers. The governing equations may be written as [2]:

$$\frac{\partial[(\rho C)_i T]}{\partial t} = \frac{\partial}{\partial y}\left(k_i \frac{\partial T}{\partial y}\right) + \mathbf{f_i} C_{R0} H_R (1-v_i)\frac{\partial \epsilon}{\partial t} + \mathbf{g_i}\varphi_c \left(\frac{I}{A}\right)^2;$$

$$i = B, F, C, T;$$

$$\mathbf{f_B} = \mathbf{f_T} = 0, \quad \mathbf{f_F} = \mathbf{f_C} = 1; \quad \mathbf{g_B} = \mathbf{g_F} = \mathbf{g_T} = 0, \quad \mathbf{g_C} = 1 \qquad (1)$$

where C_{R0} is the initial concentration of the reactive resin, H_R is the heat of reaction due to cure, I is the current flowing through conductive layers with cross-sectional area A, $(\rho C)_i$ and k_i are the volumetric specific heat and the thermal conductivity of the i^{th} material, and the subscript i denotes the different material regions in the problem domain as follows: B is the base plate, F is the resin-saturated reinforcement fiber layers, C is the resin-impregnated conductive layers, and T is the top plate. The fiber volume fraction in the i^{th} material is denoted as v_i and has significance only for $i=F$ and C. The terms $\mathbf{f_i}$ and $\mathbf{g_i}$ are binary variables (having value of 0 or 1) and signify the presence or absence of the internal heat generation due to exothermic chemical reaction and the resistive heating at specific spatial locations, respectively. In the base plate and top plate regions, $\mathbf{f_B}=\mathbf{f_T}=\mathbf{g_B}=\mathbf{g_T}=0$ which denotes the absence of internal heat generation, implying a purely conductive heat transfer. In the resin-saturated reinforcement fiber layers region, $\mathbf{f_F}=1$ while $\mathbf{g_F}=0$ which reflects the presence of exothermic cure reaction in the region. Similarly, in the region of the resin-saturated conductive mats, $\mathbf{f_C}=\mathbf{g_C}=1$ the presence of heat generation resulted from chemical reaction and resistive heating combined. The terms T, t, and y are, respectively, the temperature, time and the distance from the bottom plate along the vertical axis. The electrical resistivity of the resin-saturated conductive mats, φ_C, is evaluated based on the relation between electrical resistivity and thermal conductivity according to Lorenz law [11],

$$\frac{\varphi_C}{\varphi_{CF}} = \frac{k_{CF}}{k_{CI}} \qquad (2)$$

where φ_{CF} and k_{CF} respectively denote the electrical resistivity and thermal conductivity of the pure conductive fiber material, while k_{CI} denotes the in-plane thermal conductivity of the resin-saturated conductive mat. In this study, the conductive mats are considered to be of the plain weave architecture, where the values of the in-plane and transverse thermal conductivities, k_{CI} and k_C, are obtained using the mosaic model proposed by Ning and Chou [12,13].

The rate of cure reaction, $\partial\epsilon/\partial t$, appearing in the energy equation, Eq. (1), is modeled using an empirical expression following the approach adopted in the literature [4,5]. The kinetics of an autocatalytic cure reaction is often described in terms of an Arrhenius type rate equation as follows:

$$\frac{\partial \epsilon}{\partial t} = \left[K_{10}\exp\left(-\frac{E_1}{RT}\right) + K_{20}\exp\left(-\frac{E_2}{RT}\right)\epsilon^m\right](1-\epsilon)^n \qquad (3)$$

where ϵ is the degree of cure, defined as the fraction of the initial resin concentration, C_{R0}, that has reacted, such that $\epsilon=0$ corresponds to unreacted initial mixture, while $\epsilon=1$ denotes completion of the cure reaction. The coefficients K_{10} and K_{20} are frequency factors, E_1 and E_2 are activation energies, and R is the universal gas constant, while m and n are empirical exponents. Equation (3) models the cure of many practical resin systems, including all of the resin systems used in this study. The exact values of the corresponding kinetic parameters are presented later in this paper.

The governing equations, Eqs. (1) and (3), are solved simultaneously, subject to the following initial and boundary conditions.

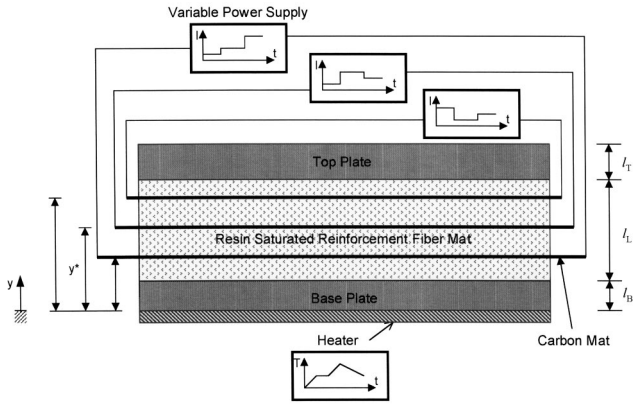

Fig. 1 A curing process configuration with embedded resistive heating elements

The initial temperature is set to be at the room temperature, T_0, while initially, the resin is completely unreacted, corresponding to $\epsilon=0$. These conditions are stated as:

$$T(y,0)=T_0, \quad (0\leqslant y\leqslant l_B+l_L+l_T)$$

$$\epsilon(y,0)=0, \quad (l_B\leqslant y\leqslant l_B+l_L) \tag{4}$$

where l_B, l_L, and l_T are the thickness of the base plate, the laminate, and the top plate, respectively as shown on Fig. 1. The temperature at the bottom of the base plate corresponds to the prescribed temperature cycle, while convective heat transfer occurs at the exposed surface of the top plate. These boundary conditions can be expressed as:

$$T(0,t)=T_B(t) \tag{5}$$

$$-k_T\frac{\partial T}{\partial y}(l_B+l_L+l_T,t)=h_T\,T(l_B+l_L+l_T,t)-T_0 \tag{6}$$

A numerical simulator was created based on the model presented above. The governing equations along with their boundary conditions were solved using an implicit one-dimensional finite-difference scheme with a control volume formulation [14,15]. The mesh consisted of 50–59 numerical grids along the *y*-direction, depending on the number of embedded conductive mats, n_C; the time step Δt was determined such that the mesh Fourier number, $\alpha\Delta t/\Delta x^2$ based on the thermal diffusivity α of every material in the domain, was less then unity. The stopping criterion for the numerical simulation was based on one of two factors namely, all sections of the laminate attained a desired minimum degree of cure, or the end of the specified cure temperature cycle was reached; the corresponding time was the cure time for the process. In addition to the cure time, t_{cure} and the minimum degree of cure, $\epsilon_{\min}$, the process model also yielded the values for the maximum temperature, $T_{\max}$, the maximum temperature gradient, $\dot{T}_{\max}$, and the maximum temperature difference, $\Delta T_{\max}$, within the laminate during the process. These values were used as the constraints in the optimization problem described in the following section. The numerical simulator, therefore, constituted the basis of the optimization problem.

3 The Optimization Problem

The objective of the optimization is to determine the temperature cycles, current cycles, and the location of the conductive mats, for minimizing the time for curing composites using embedded resistive heating elements. The optimization is subject to physical constraints on the temperature-related parameters and the degree of cure during the process. The cure temperature cycles are expressed as a series of piecewise linear segments, as presented schematically in Fig. 2. A temperature cycle is represented by the end point temperatures T_i of each stage and the respective stage durations t_i. In this study, the temperature cycles consist of four stages, which provide for a reasonably accurate representation of cure temperature schedules yet maintaining the number of decision variables sufficiently small to minimize computational effort for the optimization. Additional stages may be introduced albeit at the computational expense associated with the increased number of decision variables in the optimization.

The cure temperature cycle is represented in the optimization problem in terms of 8 decision variables: the end-point temperatures of the four stages T_1, T_2, T_3, T_4, and their corresponding stage time durations t_1^T, t_2^T, t_3^T, and t_4^T. On the other hand, the current cycles are expressed as a series of three piecewise constant segments, as shown in Fig. 2, and are represented in terms of the stage currents I_1, I_2, I_3, and the respective stage durations t_1^I, t_2^I, t_3^I. However, the cure process requires that both temperature and current cycles complete at the same time: $\Sigma_i t_i^T=\Sigma_j t_j^I$. To achieve this requirement, the last stage duration of the current cycle, t_3^I, is chosen to be a dependent variable whose value can be

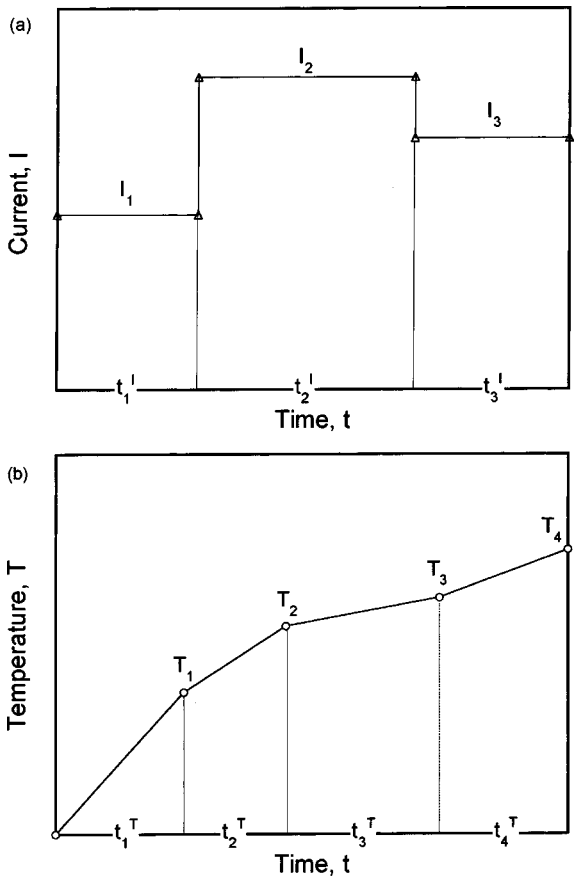

Fig. 2 Illustration of (*a*) the three-stage piecewise constant cure current cycle and (*b*) the four-stage piecewise linear curve temperature cycle considered in the study

calculated in terms of the other stage durations, as $t_3^I=\Sigma_i t_i^T-(t_1^I+t_2^I)$. Thus, in the optimization problem, t_3^I is not included as a decision variable, and the current cycle is represented in terms of 5 decision variables. Additionally, decision variables representing the locations of the conductive elements were also considered part of the design problem in this study. For a configuration with multiple embedded conductive elements, the study allows for different current cycles to be prescribed in each conductive element. Consequently, the number of decision variables is $8+6n_C$, which increases with the number of embedded conductive elements, n_C.

The objective function to be minimized is the cure time t_{cure} and the optimized variables are the parameters that comprise the temperature cycle $T_j(t_j^T)$, $j=1,\ldots,4$, the current cycle $I_k(t_k^I)$, $k=1,\ldots,3$, and the locations of the n_C conductive mat(s) y_i^*, $i=1,\ldots,n_C$. Thus, the optimization may be written mathematically as:

$$\underset{T_j(t_j^T),I_k(t_k^I),y_i^*}{\text{Minimize}} \quad t_{\text{cure}} \tag{7}$$

subject to

$$g_1=T_{\max}-T_{\text{crit}}\leqslant 0 \tag{8}$$

$$g_2=\dot{T}_{\max}-\dot{T}_{\text{crit}}\leqslant 0 \tag{9}$$

$$g_3=\Delta T_{\max}-\Delta T_{\text{crit}}\leqslant 0 \tag{10}$$

$$g_4=\epsilon_{\text{crit}}-\epsilon_{\min}\leqslant 0 \tag{11}$$

where the subscripts max, min, and crit refer to the maximum, minimum, and critical values, respectively. The temperature-related constraints [Eqs. (8)–(10)] pertain to limiting the residual/

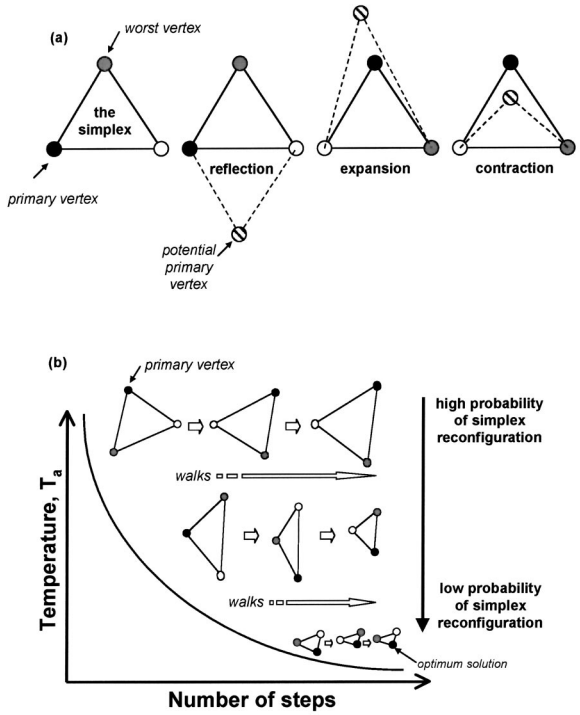

Fig. 3 Schematic diagram of simulated annealing optimization combined with simplex search algorithm

thermal stresses induced during processing, as well as to maintaining temperature and property homogeneity across the section. Constraint Eq. (11) ensures curing of composite to a desired minimum degree, ϵ_{crit}.

The optimization problem represented by Eqs. (7)–(11) was solved using the Nelder-Mead simplex method [16] combined with a simulated annealing technique to improve the effectiveness of the search [17]. The simplex method is an algorithm that performs continuous search for selecting a new point during an optimization iteration which guarantees objective function improvement. A simplex is defined as a convex hull of $N+1$ vertices in an N-dimensional space, representing the N decision variables that govern the objective function evaluation. The vertices are ranked, from best to worst, based the corresponding objective function evaluations, and the best vertex is defined as the primary vertex. Since a primary vertex represents a set of decision variables which corresponds to the lowest objective function evaluation, the finding of a new primary vertex constitutes an improvement to the objective function evaluation. Thus, the algorithm searches for a new simplex by replacing the worst vertex by a potential new primary vertex, through a set of predefined simplex movements, which include reflection, expansion, and contraction, illustrated in Fig. 3(*a*) for a two-dimensional simplex. The primary movement is the reflection of the worst vertex, while expansion and contraction are secondary movements dependent on the result of the reflection. If the reflection results in a new vertex that is better than the current primary vertex (i.e., has a lower objective function value), an expansion of the reflected simplex will follow, recognizing that a further movement of the new vertices in the direction of the reflection might lead to a much better vertex. If the reflection of the worst vertex does not lead to a new vertex that is better than the current primary vertex but still better than the next worst vertex, the new simplex is accepted. However, if the reflection of the worst vertex does not result in a vertex that is better than the next worst vertex, contraction of the original simplex is executed to reduce its size. Additional details on the Nelder-Mead algorithm, including parameter selection for the various movement and tie-breaking rules (if two vertices of equal objective function value are evaluated), may be found in Ref. [18].

In the Nelder-Mead method, the decision to accept or reject each movement is made based solely on the criterion of reducing the objective function value. This could potentially result in the entrapment of the solution in a local minimum. However, if the Nelder-Mead method were combined with a simulated annealing technique, the moves in the design exploration will be subject to a probabilistic acceptance criterion (the Metropolis equation), which offers a better opportunity to arrive at a global minimum. The optimization approach in the present application, therefore, uses a combined Nelder-Mead simplex method and simulated annealing algorithm, as discussed below.

Simulated annealing is an optimization technique which mimics the physical process of annealing (slow cooling) of metals [19], in which the molecules are free to move at high temperatures, but as the annealing temperature slowly decreases, the molecular movement becomes increasingly restricted before finally settling down to a configuration of the lowest energy state. Relating to the optimization problem, the molecular configuration represents the decision variables, while the energy state represents the objective function to be minimized. Starting at high temperature in the annealing schedule, an initial trial simplex undergoes reconfigurations based on the movements defined in the Nelder-Mead method. Each reconfiguration of the simplex is accepted based on an associated probability p, given by the Metropolis criterion [20]

$$p = \min\left(\exp\left[-\frac{E_{n+1} - E_n}{k T_a} \right], 1 \right) \tag{12}$$

where T_a is the annealing temperature, k is the Boltzmann constant, E_n is the objective function corresponding to the primary vertex prior to reconfiguration, and E_{n+1} is the objective function corresponding to the new primary vertex in the reconfigured potential simplex. If $E_{n+1} < E_n$, the probability of acceptance is unity, as per Eq. (12), which implies that a reconfiguration resulting in a lower objective function value is always accepted. In addition, Eq. (12) also allows for an occasional acceptance of an uphill move (i.e., $E_{n+1} > E_n$), based on the corresponding probability, p. The probability of accepting an uphill move is greater at higher annealing temperature T_a, while as T_a decreases the probability becomes progressively smaller.

A simplex reconfiguration following the foregoing procedure is defined as a walk. At every annealing temperature, T_a, a certain number of walks are executed before the temperature decreases according to the prescribed annealing schedule. Thus, the annealing schedule and the number of walks at each temperature constitute parameters of the simulated annealing optimization. The overall integration of the simulated annealing algorithm with the Nelder-Mead simplex method is presented in Fig. 3(*b*). Initially, at higher annealing temperature, the simplex undergoes reconfiguration at a higher probability according to Eq. (12), which in turn allows the simplex to explore more of the design domain. As the number of steps increases, the cumulative effect of the various simplex movements reduces the size of the simplex, and simultaneously, the annealing temperature also decreases, which reduces the probability of simplex reconfiguration. Near the end of the schedule, the low annealing temperature causes the probability of accepting an uphill move to be extremely low. The simplex movements continue until the algorithm reaches a stopping criterion, which is either the annealing schedule has been completed (in terms of a specified maximum number of walks), or the simplex reduces to a pre-determined infinitesimal size. The maximum number of walks can be determined in proportion to the number of decision variables [17], or by trial runs to yield an expected rate of convergence. At the stopping point, the decision variable values corresponding to the primary vertex of the simplex constitute the optimum solution.

The Nelder-Mead simplex method combined with simulated annealing is designed to solve non-linear unconstrained optimization. Since the optimization problem in hand has several constraints, g_k [Eqs. (8)–(10)], those constraints are incorporated using a penalty method [21] into an augmented objective function to be minimized, such that the optimization problem becomes unconstrained:

$$\underset{T_j(t_j^T),I_k(t_k^I),y_i^*}{\text{Minimize}} \quad t_{\text{cure}} + \sum_k \lambda_k \max(g_k,0) \tag{13}$$

where λ_k are the penalty coefficients, whose values were selected for each constraint equation g_k such that if the constraint was not satisfied the constraint penalty contributed, $\lambda_k g_k$ is equal to 100 times the expected value of the optimal cure time. If the constraint g_k is satisfied, $\max(g_k,0)$ evaluates to zero, since g_k is negative, and constraint g_k does not contribute to the penalty.

As described previously, the number of decision variables in the optimization problem varies depending on the number of conductive mats, n_C. For example, optimization of a process with one embedded carbon mat would require 14 decision variables: 8 variables representing temperature cure cycles, 5 variables representing one current cycle, and one variable for the location of the mat. Thus, the simplex is formed in a 14-dimensional space, and consisted of 15 vertices. The initial guess on the values of the decision variables corresponds to one of the vertices of the simplex, and the other 14 vertices are created by adding scaled basis unit vectors $\beta \mathbf{e}_{(\mathbf{n})}$—where β is a scaling factor, such that the hypersurfaces of the simplex are linearly independent of each other. The numerical process simulator is invoked to determine the augmented objective function corresponding to each vertex at every step of the optimization procedure. At the completion of the optimization algorithm, the primary vertex of the final simplex represents the optimal decision variables, and the corresponding objective function evaluation represents the optimal cure time, t_{cure}^*.

4 Results and Discussion

The optimization approach presented in the previous section was validated in two parts: First, the numerical simulation model, which forms the core of the framework, was validated with experimental data on a variety of resistive heating configurations. The validation results are presented in Ref. [2] and are not repeated here. Secondly, the optimization framework utilizing the process model was validated using the results presented in Ref. [2]. In their study, the process consisted of a fixed cure temperature cycle, and a steady current was used for the resistive heating. Parametric investigations were conducted by varying the number of embedded heating elements, and the resin kinetics parameters [for kinetics of the form in Eq. (3), but with $K_{10}=0$]. The parametric results were used to derive the optimum resistive heating configurations that minimized the cure time while satisfying constraints of the form in Eqs. (8)–(11). The results were expressed in terms of a dimensionless power density, P_d, defined as $P_d = (l_L^2 \varphi_C / T_0 k_L)(I/A)^2$, and dimensionless groups representing the kinetics parameters.

For the purpose of validation, the current cycle in the present formulation was taken to be a single stage, and the cure temperature cycle was fixed to be that used in Ref. [2]. Furthermore, the carbon mat locations were prescribed to be the values used in Ref. [2]. Thus, the decision variable in the optimization was reduced to only the stage current magnitude. The optimization framework was used to solve for the optimal steady current, for varying resin kinetics parameters, subject to the same critical values of the constraint parameters [Eqs. (8)–(11)] as in Ref. [2]. Figure 4 shows an example comparison of the variation of the optimal current, expressed as a dimensionless power density, P_d, with the Damköhler number, Da—a dimensionless group which signifies the ratio of the conduction time scale to the reaction time scale—defined as $\text{Da}=K_{20} l_L^2/\alpha_L$, where α_L is the thermal diffusivity of the laminate. The plot corresponds to three embedded heating elements, and shows that the optimal dimensionless power density increases with the Damköhler number. Overall, the optimization results (markers in the plot) are seen to correspond closely to the results from Ref. [2] derived using parametric studies (shown as the dashed line).

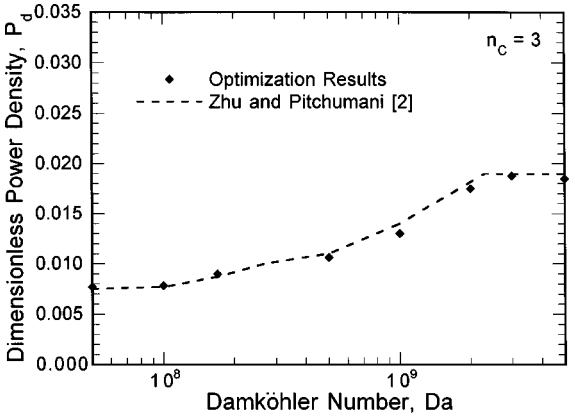

Fig. 4 Validation of the optimization results with the data from Ref. [2], for the resistive heating configuration using three carbon mats

With the validated optimization framework as basis, the optimization studies presented in this paper focus on three material systems: a fiberglass-epoxy resin system EPON 815 catalyzed with EPICURE-3274, an Owens-Corning fiberglass-polyester system with Percadox 16N and benzoyl peroxide initiator (OC-E701/P16N/BPO) and a polyester system, CYCOM-4102 of American Cyanamid Company. The embedded resistive heating elements are considered to be carbon mats, G-104, of Textile Technologies Inc. The reaction kinetics for the resin systems are summarized in Table 1, and the physical properties of the material systems are also available in the references cited in Table 1. The tooling plate considered in the study is made out of copper with volumetric specific heat $(\rho C)_T$ of 3439.2 kJ/m^3 K, and thermal conductivity (k_T) of 395.0 kW/m K.

Optimization runs are carried out for fixed number of carbon mats n_C, by initially supplying trial values of the cure temperature cycle, the current cycle through each carbon mat, and the location of the carbon mat(s) across the thickness. The critical values of the constraint used in the study are set to be identical for all material systems, as follows:

$$T_{\text{crit}}=150°\text{C}; \quad \dot{T}_{\text{crit}}=0.6°\text{C/s}; \quad \Delta T_{\text{crit}}=69°\text{C}; \quad \epsilon_{\text{crit}}=0.97 \tag{14}$$

These values typify those commonly required in practice. However, the effect of varying constraint values is also investigated later in this section. The optimization procedure is executed until the optimal cure time, and the corresponding temperature cycle, current cycles, and carbon-mat locations, have been found. Each optimization run was repeated for ten different initial trial solutions, and the optimum results corresponding to the least cure time value among the ten trial results was taken to be the global optimum solution. In most cases, it was observed that the global optimum solution was reached in several of the ten trials.

Figure 5 shows the optimal temperature cycles, in solid lines, and the optimal current cycles, in dashed lines, as well as the optimal locations of carbon mats (y^*) for curing a 1.27 cm-thick fiberglass/EPON-815/EPICURE-3274 system with different numbers of embedded carbon mats, n_C. The optimal cure time for the process without resistive heating is 1710 seconds (Fig. 5(*a*)). The optimal cure times for n_C carbon mats, $t_{n_C}^*$, nominally reduces as the number of carbon mats increases: 1002 seconds for 1 mat (Fig. 5(*b*)), 961 seconds for 2 mats (Fig. 5(*c*)), and 948 seconds for 3

Table 1 Kinetics model and parameters for systems used in the study

Material	Kinetics Model	Kinetic Parameters
CYCOM-4102 Pillai et al. [3]		$K_{10}=0\ \text{min}^{-1}$ $K_{20}=3.7\times10^{22}\ \text{min}^{-1}$ $E_1=0$ kJ/kmol $E_2=1.66\times10^5$ kJ/kmol $H_R=74.1$ kJ/kg $m=0.524;\ n=1.476$
OC-E701/P16N/BPO Han et al. [5]	$\frac{d\varepsilon}{dt}=(K_{10}e^{-E_1/RT}+K_{20}e^{-E_2/RT}\varepsilon^m)(1-\varepsilon)^n$	$K_{10}=5.69\times10^{12}\ \text{s}^{-1}$ $K_{20}=8.61\times10^8\ \text{s}^{-1}$ $E_1=1.07\times10^5$ kJ/kmol $E_2=7.51\times10^4$ kJ/kmol $H_R=200$ kJ/kg $m=0.58;\ n=1.42$
EPON-815/EPICURE-3274 Ramakrishnan et al. [1]		$K_{10}=0\ \text{s}^{-1}$ $K_{20}=4.18\times10^5\ \text{s}^{-1}$ $E_1=0$ kJ/kmol $E_2=55.92$ kJ/kmol $H_R=384$ kJ/kg $m=0.25;\ n=1.75$

mats (Fig. 5(*d*)). Compared to the optimal cure time without resistive heating, the presence of one carbon mats reduces the optimal cure time by about 41 percent, which is a significant improvement in the processing time. However, the cure time reduction by further addition of carbon mats is somewhat small in proportion to the actual cure time, thus implying that for EPON-815/EPICURE-3274, increasing the number of carbon mats beyond 1 is seen to be less economical considering the cost associated with the additional carbon mats. This points to one carbon mat being the practically optimal solution. The optimal location for the single carbon mat is at $y^*=1.22$ cm, which is near the top plate. For the cases with two and three carbon mats (Figs. 5(*c*) and 5(*d*), respectively), the optimal location of one of the carbon mats is also at the identical location, $y^*=1.22$ cm. This result confirms the intuitive notion that any additional heat source must be first located farthest from the peripheral heating to obtain the optimum solution.

The variation of the optimal number of carbon mats with the kinetic properties of the material system is examined by considering the OC-E701/P16N/BPO and CYCOM-4102 resin systems which exhibit faster kinetics relative to EPON-815/EPICURE-3274. Figures 6 and 7 present the results for OC-E701/P16N/BPO and CYCOM-4102, respectively. Without resistive heating the optimal cure times are 1172 seconds for OC-E701/P16N/BPO and 3012 seconds for CYCOM-4102 (Figs. 6(*a*) and 7(*a*)). Using one carbon mat, $n_C=1$, the optimal cure time reduces to 418 seconds for OC-E701/P16N/BPO and 742 seconds for CYCOM-4102, which constitute savings of 64 percent and 75 percent, respectively, compared to the respective cure times without resistive heating. The Figures show that as the number of carbon mats increases from $n_C=1$ (Figs. 6(*b*) and 7(*b*)) to $n_C=2$ (Figs. 6(*c*) and 7(*c*)), a significant further reduction in optimal cure time is achieved for both material systems: 334 seconds ($n_C=2$) for OC-E701/P16N/BPO, and 509 seconds ($n_C=2$) for CYCOM-4102. However, as the number of mats increases to $n_C=3$ (Figs. 6(*c*) and 7(*c*)), the cure time reduction becomes less relative to that of going from $n_C=1$ to $n_C=2$: 325 seconds for OC-E701/P16N/BPO and 487 seconds for CYCOM-4102, implying that two carbon mats can be considered the practically optimal configuration

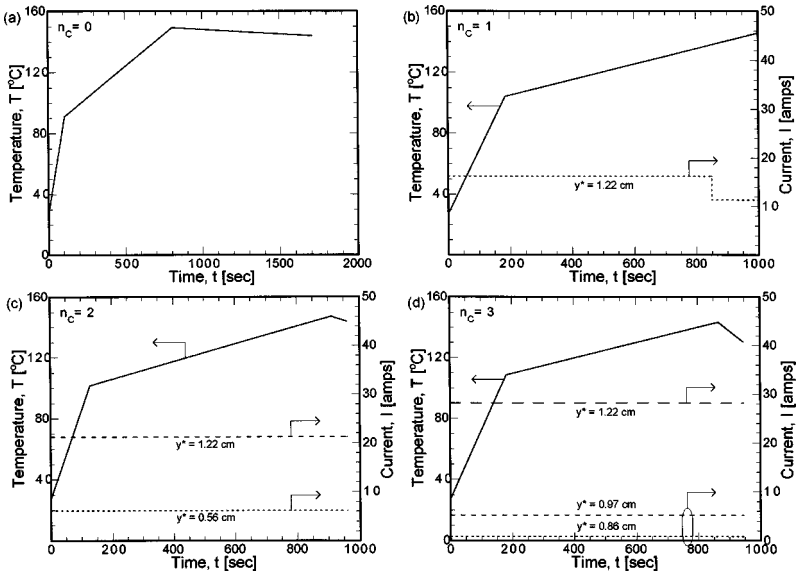

Fig. 5 Optimal temperature and current cycles for curing a 1.27 cm-thick EPON-815/EPICURE-3274 laminate embedded with (*a*) 0 carbon mat, (*b*) 1 carbon mat, (*c*) 2 carbon mats, and (*d*) 3 carbon mats

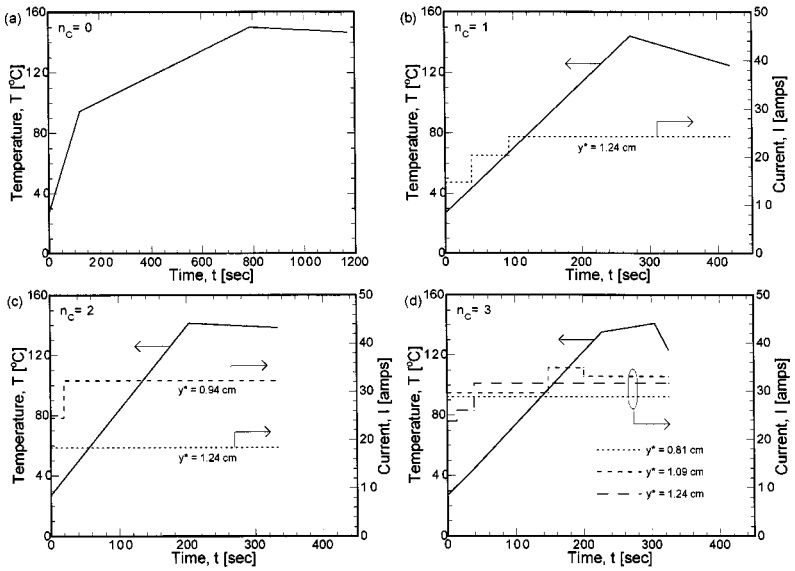

Fig. 6 Optimal temperature and current cycles for curing a 1.27 cm-thick OC-E701/P16N/BPO laminate embedded with (*a*) 0 carbon mat, (*b*) 1 carbon mat, (*c*) 2 carbon mats, and (*d*) 3 carbon mats

for both material systems. This result, together with the case of EPON-815/EPICURE-3274 discussed above, shows that as the reactivity of the material system increases, the optimal number of mats also increases. This trend was also reported based on parametric studies in Ref. [2].

It is worth examining the form of the optimal temperature cycles (solid lines) and the current cycles (dashed lines) relative to the constraints in the optimization. In the case of $n_C=1$, the gradual increase via multiple steps to higher current value in the current cycles shown in Figs. 6(*b*) and 7(*b*) may be attributed to the temperature gradient constraint which limits the sudden increase in temperature due to resistive heating by high current near the top surfaces. However, in the case of EPON-815/EPICURE-3274 in Fig. 5(*b*), the current stays constant at a lower value through the process before it drops at the end of the cure cycle, thereby satisfying all the constraints. In the multiple-carbon-mat cases, $n_C=2$ and $n_C=3$, the gradual increase in the current cycles does not exist due to additional heat sources inside the laminates which allows more homogeneous increase of temperature—thereby maintaining temperature difference below the critical value—throughout the laminate. This allows more heat to be supplied to the laminates since the beginning of the cycle without violating any constraint, thus enabling a faster cure process.

As discussed above, the critical values of the constraints affect closely the shape of the cure cycles and, in turn, the optimal cure time. Toward elucidating this effect further, studies were conducted to investigate the effect of the critical values of the constraints on the optimal cure temperature and current cycles. Figure 8(*a*) presents the result for a reference set of critical values for the case of curing a 1.27 cm-thick CYCOM-4102, while Figs. 8(*b*), 8(*c*), and 8(*d*) present the temperature cycles, in solid lines, and current cycles, in dashed lines, for different values of T_{crit}, ΔT_{crit},

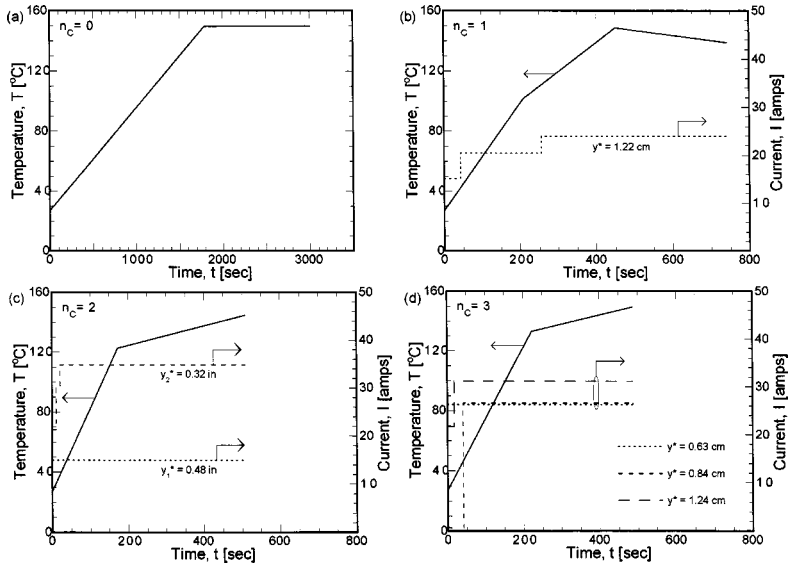

Fig. 7 Optimal temperature and current cycles for curing a 1.27 cm-thick CYCOM-4102 laminate embedded with (*a*) 0 carbon mat, (*b*) 1 carbon mat, (*c*) 2 carbon mats, and (*d*) 3 carbon mats

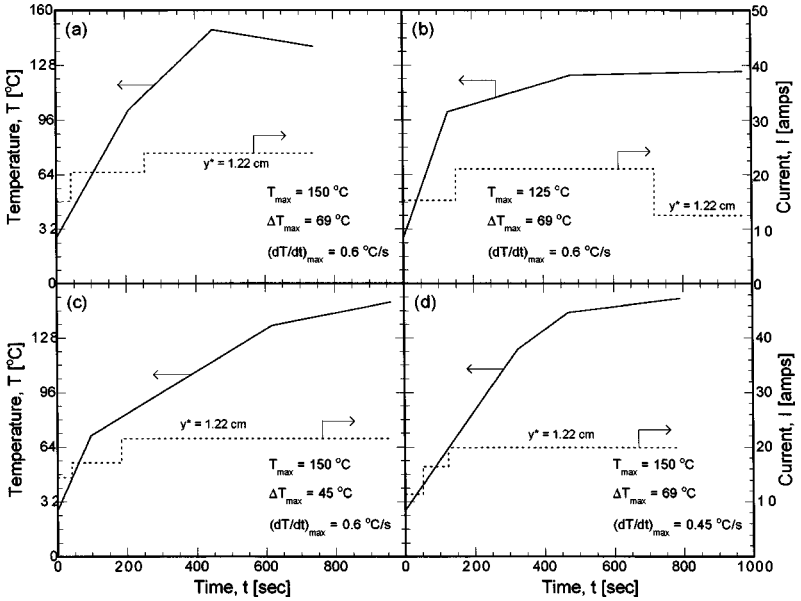

Fig. 8 Optimal temperature and current cycles for curing a 1.27 cm-thick CYCOM-4102 laminate embedded with 1 carbon mat for different critical values of constraints

and $\dot{T}_{\text{crit}}$, respectively. In all these cases, resistive heating using one carbon mat was considered. Figures 8(*a*) and 8(*b*) demonstrate that the optimal cure time increases as the critical temperature, T_{crit}, constraint is tightened. The corresponding temperature and current cycles demonstrate variations to accommodate the smaller value of critical temperature, highlighted by a step decrease in the current cycle at the end of the curing process. Figures 8(*c*) and 8(*d*) suggest that as the constraints of critical temperature difference and critical temperature gradient are tightened, the optimal cure time, $t^*_{n_C}$, increases as expected due the fact that as both constraints limit the rate of temperature increase, the cure process requires longer time to complete. Further, Fig. 8(*c*) shows that as the allowable temperature difference, ΔT_{crit} decreases, the optimal temperature cycle is adjusted to provide slower temperature ramps. Figure 8(*d*) also reveals that a smaller value of the allowable temperature gradient $\dot{T}_{\text{crit}}$ causes the current cycle to start from a lower initial value to avoid excessively rapid heating rate.

To further illustrate the effects of tighter constraints on the optimal curing process in the presence of resistive heating, the temperature history at selected locations within the laminate are presented in Fig. 9, which refers to a 1.27 cm-thick CYCOM-4102 system with one embedded carbon mat, $n_C = 1$, at optimal location $y^* = 1.22$ cm. Figure 9(*a*) shows the optimal current cycle (bold line) and the temperature history at three different locations across the thickness (thin lines), corresponding to a critical temperature, T_{crit}, of 150°C. The temperatures near the base plate ($y = 0$ cm) are similar to the prescribed temperature cycle, as seen in Fig. 8(*a*). Without resistive heating element, the temperatures near the top surface ($y = 1.27$ cm) would be lower than those at other locations within the laminate. However, the presence of a carbon mat near the top surface causes the temperatures in the middle of the laminate ($y = 0.635$ cm) to be the lowest across the section, for this case considered. Figure 9(*a*) also verifies that the magnitude of the increase in the current cycle is governed by the temperature gradient constraint, since an increase in current cycle magnitude causes rapid temperature change near the carbon mat at that instant, as seen in the temperature history at $y = 1.27$ cm, corresponding to various steps in the current cycle ($t \approx 50$ s and $t \approx 250$ s). Figure 9(*b*) presents the temperature history plot for critical temperature, $T_{\text{crit}} = 125$°C, showing that a decrease in the magnitude of electrical current at the later stage of the curing process is necessary to avoid violating the critical temperature constraint. Near the top surface ($y = 1.27$ cm), where the carbon mat is located, the temperature variation exhibits a brief reversal in the increasing trend to that of decreasing at the time the current

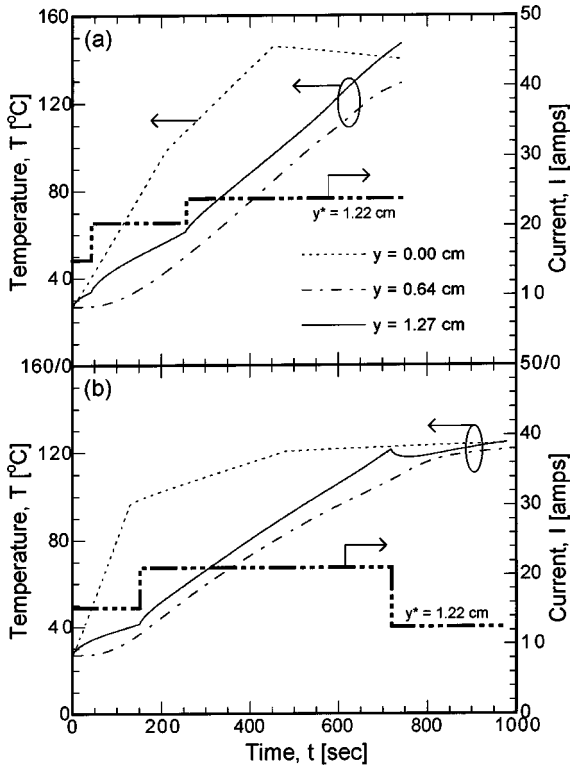

Fig. 9 Temperature history at various locations within the laminate during curing process using the optimal temperature and current cycles for a 1.27 mm-thick CYCOM-4102 laminate, for critical temperatures of: (*a*) 150°C and (*b*) 125°C

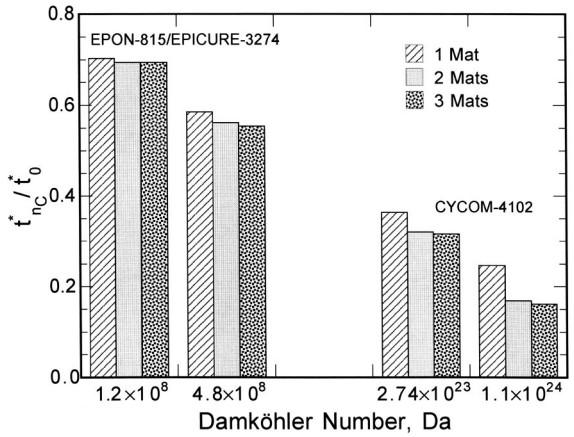

Fig. 10 Normalized optimal cure time as a function of dimensionless Damköhler number

magnitude is reduced, $t \approx 700$ sec, thereby allowing the process to continue without violating the constraint on maximum temperature.

Considering the issue of optimal number of mats, n_C^*, for different material systems, it is helpful to summarize the results as a function of the Damköhler number, Da. Figure 10 presents a summary of the optimal results for two different materials for which the kinetics model has only one pre-exponential factor and one activation energy (Table 1). The Damköhler number is defined based on this non-zero pre-exponential factor as $K_{20}l_L^2/\alpha_L$. The variation in the Damköhler number within each material system is obtained by changing the laminate thickness, whereas the variation of Da from one material system to another reflects the change in the pre-exponential factor. The *y*-axis of the plot represents the ratio between the optimal cure time for curing with n_C carbon-mats, $t^*_{n_C}$, and the optimal cure time without resistive heating, t_0^*, and is a measure of the savings in the cycle time due to resistive heating. The Figure shows that as Da increases, which corresponds to reduced reaction time scale relative to heat diffusion time scale, the value of the cure time ratio decreases, which translates to an increase in the savings in optimal cure time by using resistive heating. This may be attributed to the fact that as the reactivity of the resin increases, the presence of resistive heating elements helps expedite the curing process to a greater extent. The Figure further shows that as the number of mats increases, the optimal cure time decreases as also noted previously. It may be reasoned that while incorporation of additional carbon mats progressively reduces the optimal cure time, the savings in cure time has to be viewed relative to the cost/effort of inclusion of more heating elements. For larger values of Da, increasing the number of carbon mats from one to two significantly reduces the cure time, while the effect of increasing from two to three carbon mats is seen to be much less significant on the cure time savings, despite an absolute decrease in the optimal cure time. For smaller Damköhler numbers, Fig. 10 shows that even an increase in n_C from 1 to 2 offers less of savings in cure time.

In an attempt to determine the optimal number of carbon mats, n_C^*, a cost analysis in terms of both cure time and power usage comparison is presented in Fig. 11. The power consumption is calculated in this study as:

$$P_{n_C} = \sum_{i=1}^{n_C} \int_0^{t^*_{n_C}} I_i(t)^2 dt \tag{15}$$

The Figure presents, as a stacked bar plot, the normalized cure time savings, $\tau_{n_C} = (t_0^* - t^*_{n_C})/t_0^*$, and the normalized power savings, $P^*_{n_C} = (P_{\max} - P_{n_C})/P_{\max}$, for different number of carbon

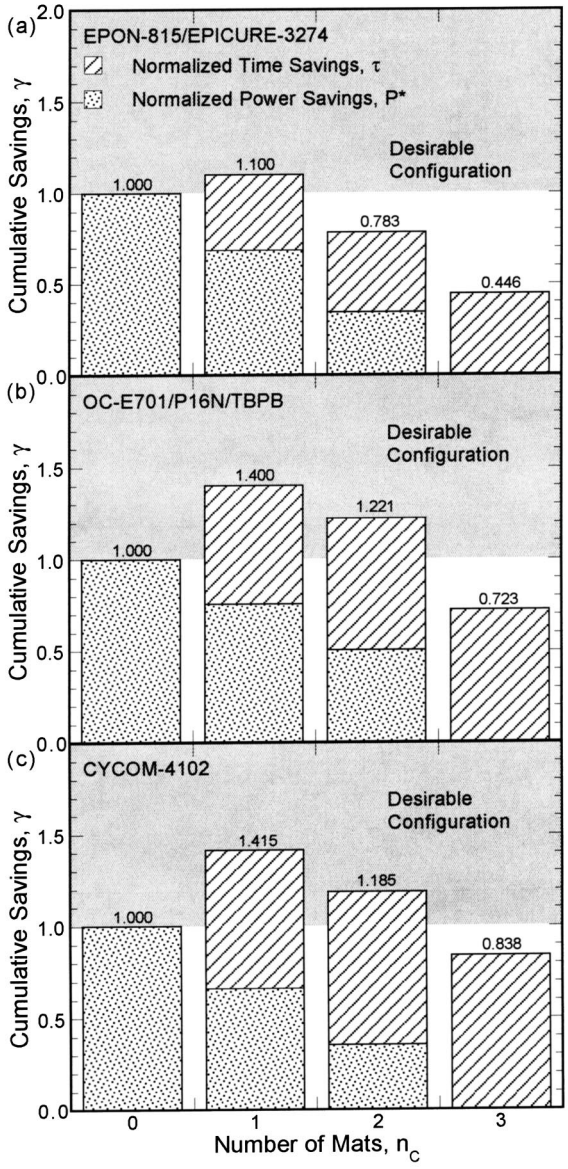

Fig. 11 Normalized cure time and power consumption savings as a function of number of carbon mats, for (*a*) EPON-815/EPICURE-3274, (*b*) OC-E701/P16N/BPO, and (*c*) CYCOM-4102

mats, n_C, for all material systems used in this study. The maximum power, $P_{\max}$, corresponds to the power consumption for $n_C = 3$ for each material system. The sum of the normalized cure time savings and the normalized power savings is referred to as the cumulative savings parameter, γ_{n_C}. For the processing without resistive heating ($n_C = 0$): $\tau_0 = 0$ and $P_0^* = 1$ independent of material system, which leads to $\gamma_0 = 1$. It follows that for the processing with resistive heating, it is desirable that the cumulative savings exceed that for the reference case of no resistive heating, i.e., $\gamma_{n_C} > \gamma_0$. Since $\gamma_0 = 1$, the region $\gamma_{n_C} > 1$ is identified in the plots as the desirable configuration for resistive heating. This region is indicated by the shaded area in Figs. 11(*a*)–11(*c*). Based on the consideration of time and power savings, Fig. 11 provides for deciding the number of carbon mats that constitutes the optimal configuration for each resin system. It is seen that the single carbon mat configuration offers the most cumulative savings for all the resin systems. Further, for EPON-815/EPICURE-3274 (Fig. 11(*a*)), one carbon mat is the only configuration that satisfies

$\gamma_{n_C} > 1$, while for OC-E701/P16N/BPO (Fig. 11(*b*)) and CYCOM-4102 (Fig. 11(*c*)), both one and two carbon mats satisfy the criterion. Since additional carbon mats always reduces the cure time, the optimal number of carbon mats n_C^* could be defined as the highest number of mats for which the cumulative savings exceeds that of the process without resistive heating. Thus, the optimal number of carbon mats for EPON-815/EPICURE-3274 is one, while for OC-E701/P16N/BPO and CYCOM-4102 two carbon mats constitute the optimal configuration. It may be noted from Fig. 10 that the CYCOM-4102 system corresponds to higher Damköhler number value in comparison to the EPON-815/EPICURE-3274 system for the same laminate thickness. The results in Fig. 11(*a*) and 11(*c*), therefore, suggest that the cumulative power and time savings, γ_{n_C}, increases with Damköhler number.

The paper presented a comprehensive discussion on the optimization of temperature and current cycles for curing process using resistive heating. The results in terms of optimal cure time, optimal current cycles along with optimal location and configuration provide a valuable reference for better process design. The optimization framework presented in the paper may be used to determine optimal temperature and current cycles for constraint values other than those used in the study, although the physical trends elucidated in this article are expected to be generally valid.

5 Conclusions

A systematic approach to optimization of a process for fabrication of thermosetting-matrix composites by the use of embedded resistive heating element was presented. The objective was to determine the optimal temperature cycles, electrical current cycles, and the conductive mats configuration so as to minimize the fabrication time subject to process constraints. A numerical model formed the basis of the optimization problem, which was solved using a combination of simulated annealing and simplex search algorithm. Optimal cure times, temperature and current cycles were presented for three material systems with different reaction kinetics. The optimal solutions are presented for various conductive mats configuration, as well as several process design constraints. The results showed that the approach of varying the current with time together with the cure temperature cycles leads to cure time reduction. In general, the cure time decreases as the number of mats increases, and for the material systems considered in the study, one or two carbon mats were shown to be the practical optimal configuration, based on an analysis incorporating the electrical power consumption of the resistive heating elements. The variation of the results with the resin kinetics and composite thickness were reported in terms of a non-dimensional Damköhler number, which showed that material systems with higher reactivity or larger thickness experienced greater cure time reduction by the additional resistive heating elements.

Acknowledgment

The study was funded by the National Science Foundation through Grant Nos. DMI-0119430 and CTS-0112822. The authors gratefully acknowledge the support.

Nomenclature

A = cross-sectional area of conductive mat
C_{R0} = initial concentration of the reactive resin [kg/m^3]
E_1, E_2 = activation energies in the kinetics model [kJ/mol]
E_n, E_{n+1} = energy states in simulated annealing
$\mathbf{f_i}$, $\mathbf{g_i}$ = binary variables
g_k = constraint values
h = heat transfer coefficient [W/m^{2}K]
H_R = heat of the cure reaction [kJ/kg]
I = electrical current [A]
k_{CI} = in-plane thermal conductivity of resin-saturated conductive mat
k_i = thermal conductivity of material i [W/mK]
K_{10}, K_{20} = pre-exponential factors in the kinetic model [s^{-1}]
l_i = thickness of material i [m]
m, n = empirical exponents in the kinetics model
n_C = number of carbon mats
p = probability factor in the Metropolis criterion
P^* = normalized electrical power savings
R = universal gas constant [kJ/mol K]
t = time [s]
T = temperature in the composite at any time t and spatial location y [K]
T_a = annealing temperature [K]
v_i = fiber volume fraction of material i
x, y = coordinate axes
y^* = optimal location of conductive mat [cm]

Greek Symbols

α = thermal diffusivity $k/\rho C$ [m^2/s]
γ = normalized cumulative savings
ϵ = degree of cure
φ_C = electrical resistivity of resin saturated conductive mat [Ohm/m^2]
φ_{CF} = electrical resistivity of pure conductive mat [Ohm/m^2]
ρC = volumetric specific heat [kJ/m^{3}K]
τ = normalized cure time savings

Subscripts

$*$ = optimal value
B = base plate
C = resin-impregnated conductive layer
F = resin-saturated fiber layer
L = laminate
T = tooling
crit = critical value
max = maximum value
min = minimum value
n_C = number of conductive mats

References

[1] Ramakrishnan, B., Zhu, L., and Pitchumani, R., 2000, "Curing of Composites Using Internal Resistive Heating," J. Manuf. Sci. Eng., **122**, pp. 124–131.
[2] Zhu, L., and Pitchumani, R., 2000, "Analysis of a Process for Curing Composites by the Use of Embedded Resistive Heating Elements," Compos. Sci. Technol., **60**, pp. 2699–2712.
[3] Pillai, V. K., Beris, A. N., and Dhurjati, P. S., 1994, "Implementation of Model-Based Optimal Temperature Profiles for Autoclave Curing of Composites Using a Knowledge-Based System," Ind. Eng. Chem. Res., **33**, pp. 2443–2452.
[4] Loos, A. C., and Springer, G. S., 1983, "Curing of Epoxy Matrix Composites," Journal of Composite Materials, **17**, pp. 135–169.
[5] Han, C. D., Lee, D. S., and Chin, H. B., 1986, "Development of a Mathematical Model for the Pultrusion Process," Polym. Eng. Sci., **26**, pp. 393–404.
[6] Bogetti, T. A., and Gillespie, J. W., 1991, "Two Dimensional Cure Simulation of Thick Thermosetting Composites," Journal of Composite Materials, **25**, pp. 239.
[7] Ciriscioli, P. R., Wang, Q., and Springer, G. S., 1992, "Autoclave Curing—Comparison of Model and Test Results," Journal of Composite Materials, **26**, pp. 90–103.
[8] Rai, N., and Pitchumani, R., 1997, "Optimal Cure Cycles for the Fabrication of Thermosetting-Matrix Composites," Polym. Compos., **18**, pp. 566–581.
[9] Lee, W. I., and Springer, G. S., 1984, "Microwave Curing of Composites," Journal of Composite Materials, **18**, pp. 387–409.
[10] Thostensen, E., and Chou, T.-W., 1998, "Microwave Accelerated Curing of Thick Composite Laminates," *Proceedings of the 13th American Society for Composite Conference*, Baltimore, MD, pp. 595–604.
[11] London, E. U., and Odishaw, H., 1991, *Handbook of Physics*, McGraw-Hill, New York, NY.
[12] Ning, Q., and Chou, T.-W., 1995, "A Closed-Form Solution for the Transverse Effective Thermal Conductivity of Woven Fabric Composites," Journal of Composite Materials, **29**, pp. 2280–2294.
[13] Ning, Q., and Chou, T.-W., 1995, "Closed-Form Solution for the In-Plane Effective Thermal Conductivity of Woven Fabric Composites," Compos. Sci. Technol., **55**, pp. 41–48.

[14] Patankar, S. V., 1980, *Numerical Heat Transfer and Fluid Flow*, Hemisphere, Washington, DC.
[15] Anderson, D. A., Tannehill, J. C., and Pletcher, R. H., 1984, *Computational Fluid Mechanics and Heat Transfer*, Hemisphere, Washington, DC.
[16] Nelder, J. A., and Mead, R., 1965, ''A Simplex Method for Function Minimization,'' Comput. J. (UK), **7**, pp. 308–313.
[17] Press, W. H., Flannery, B. P., Teukolsky, S. A., and Vettering, W. T., 1992, *Numerical Recipes in FORTRAN*, Cambridge University Press, New York, NY.
[18] Lagarias, J. C., Reeds, J. A., Wright, M. A., and Wright, P. E., 1998, ''Convergence Properties of the Nelder-Mead Simplex Method in Low Dimensions,'' SIAM J. Optim., **9**, pp. 112–147.
[19] Kirkpatrick, S., Gelatt, C. D., and Vecchi, M. P., 1983, ''Optimization by Simulated Annealing,'' Science, **220**, pp. 671–680.
[20] Metropolis, N., Rosenbluth, A., Rosenbluth, M., and Teller, A., 1953, ''Equation of State Calculations by Fast Computing Machines,'' J. Chem. Phys., **21**, pp. 1087–1092.
[21] Bertsekas, D. P., 1999, *Nonlinear Programming*, Athena Scientific, Belmont, MA.